Proceedings of 2nd International Symposium on Turbulent and Shear Flow Phenomena, Vol. 2,
Royal Institute of Technology (KTH), Stockholm, Sweden, June 27 - 29, 2001, pp. 519-524.

LARGE EDDY SIMULATIONS OF TURBULENT FLOW AND INCLUSION TRANSPORT IN CONTINUOUS CASTING OF STEEL

Quan Yuan, S. P. Vanka and Brian G. Thomas
Department of Mechanical and Industrial Engineering
University of Illinois at Urbana-Champaign
1206 W Green Street, Urbana, IL 61801 USA
quanyuan@uiuc.edu, s-vanka@uiuc.edu, bgthomas@uiuc.edu

ABSTRACT

Turbulent structures are important in influencing inclusion transport in continuous casting of steel. The turbulent velocity field and inclusion transport are studied in a full-scale water model using large eddy simulations. The computed fluid velocities are compared with measurements. Chaotic vortex structures were computed in the upper roll region as expected. The computed inclusion trajectories were processed to determine the inclusion removal rate to the top surface. The results agree reasonably with measurements from the water model. The removal of particle inclusions to the top surface is found to be independent of the particle initial positions at which they enter the mold.

INTRODUCTION

Turbulence plays an important role in continuous casting of steel. The transient turbulent structures in the mold region of a continuous caster influence the entrapment of the top surface flux layer and the motion of inclusion particles. The inclusions exiting the submerged entry nozzle (SEN) may either float to the top surface and get safely removed into the slag layer, or may be trapped in the solidifying front, leading to defects such as internal cracks and slivers in the final rolled product.

A number of previous studies have analyzed this flow using Reynolds-averaged turbulence models, typically the k-ε model. However, the k-ε model gives only the time-averaged transport, and at best only crudely predicts the turbulence dynamics and particle transport by turbulence.

Large Eddy Simulations (LES) of turbulence provide an attractive method for simulating turbulent flows. In comparison with the Reynolds-averaged approach, LES provides much more realistic and accurate representation of a turbulent flow by resolving the large-scale dynamics. This information is crucial in estimating the heat mass and momentum transport, and transport of inclusions. Turbulence is also important in estimating the entrapment of the flux layer on the top surface of the mold. LES has been applied in the past to model many simple turbulent flows. However, its application to a highly complex flow such as that in the mold region of a continuous caster presents many new challenges. These include prescription of the correct inlet conditions to the computational domain,adequately resolving all velocity and thermal boundary layers, simulating the two-phase flow resulting from injection of argon bubbles and inclusions, and resolving the transient solidification front. Further, experiments in water models have shown the presence of large-scale unsteadiness in the flow, which mandates long simulation times. Therefore, the computational burden of such simulations is very high.

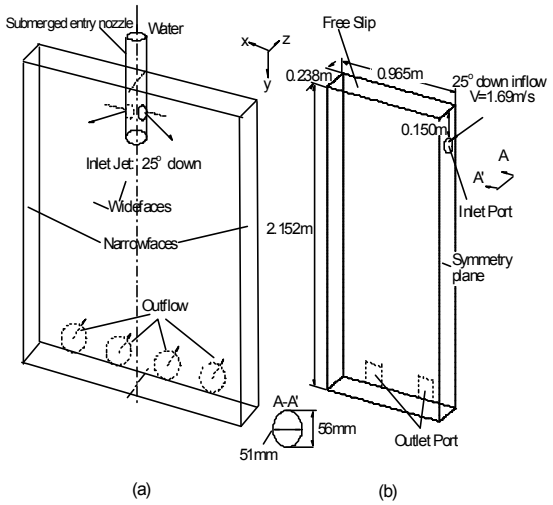

Figure 1: Schematic of (a) water model and (b) simulation domain.

Because of nearly equal kinematic viscosities of the liquid steel and water which determine the main flow characteristics, flow in the steel caster mold region can be studied using scaled water models. In the present study, we have conducted LES of the flow in a full-scale water model. Our objective is to understand the instantaneous structures in the flow and the motion of inclusion particles, and to compare the LES results with experimental data where available.

PROBLEM DESCRIPTION

Figure 1 shows an experimental set-up at AK Steel Company (Sussman, 1992), and the corresponding computational domain used to simulate this water model experiment. In the experiment, around 8000-30000 elliptical disk-shaped plastic beads were injected into the mold

Proceedings of 2nd International Symposium on Turbulent and Shear Flow Phenomena, Vol. 2,
Royal Institute of Technology (KTH), Stockholm, Sweden, June 27 - 29, 2001, pp. 519-524.

with the water through the nozzle to study the particle transport. The density and size of the beads were chosen to match the vertical terminal velocity of 300μm alumina inclusions in the liquid steel. A screen was positioned near the top surface to trap the plastic beads and thereby simulate the fraction of inclusion particles removed to the top surface. The experiments were repeated for at least five times and the averaged inclusion removal by the screen was reported (Sussman, 1992). A hot-wire anemometer was used to measure the fluid velocity field.

The LES was conducted to study the flow and particle transport for this water model to compare with the experiments and gain more insights. At the inlet, the instantaneous velocity profiles from a fully developed turbulent flow in a pipe are prescribed. The velocities are directed at an angle of 25^o downwards to the horizontal axis. Only half of the mold domain is computed at this time with the assumption of symmetry about the central plane. The computational conditions are compared with those of the experiment in Table 1. Six groups of particles were introduced from the inlet within a short time period at different times, as shown in Table 2.

MATHEMATICAL MODELING

Fluid Flow

The time-dependent three-dimensional Navier-Stokes equations have been solved for the fluid velocity field. The Smagorinsky eddy viscosity model (Smagorinsky, 1963) is used to represent the unresolved scales:

$$\frac{\partial \mathrm{v}_i}{\partial x_i} = 0 \tag{1}$$

$$\frac{D\mathrm{v}_i}{Dt} = -\frac{1}{r}\frac{\partial p}{\partial x_i} + \frac{\partial}{\partial x_j} n_{eff}\left(\frac{\partial \mathrm{v}_i}{\partial x_j} + \frac{\partial \mathrm{v}_j}{\partial x_i}\right) \tag{2}$$

$$n_{eff} = n_0 + 0.01(\Delta x \Delta y \Delta z)^{2/3}\sqrt{\frac{\partial \mathrm{v}_i}{\partial x_j}\frac{\partial \mathrm{v}_i}{\partial x_j} + \frac{\partial \mathrm{v}_i}{\partial x_j}\frac{\partial \mathrm{v}_j}{\partial x_i}} \tag{3}$$

The equations are discretized using the Harlow-Welch fraction step procedure (Robichaux, 1990) on a staggered grid. Second order central differencing is used for the convection terms and the Crank-Nicolson scheme is used for the diffusion terms. The Adams-Bashforth scheme is used to discretize in time with second order accuracy. The implicit diffusion terms are solved using Alternative Line Inversion. The pressure Poisson equation is solved using a direct Fast Fourier Transform solver. For parallelization, 1-D domain decomposition with MPI (Message Passing Interface) is utilized. The computation was conducted with a mesh consisting of 128×169×64 nodes in the x, y and z directions respectively. The time-dependent equations were integrated for 175,000 time steps (140 seconds of real time).

	Experiment	LES simulation
Nozzle port size /Inlet port size (x × y) (m)	0.051 × 0.056	0.051 × 0.056
Submergence depth (m)	0.150	0.150
Nozzle angle	25^o	25^o
Inlet jet angle	25^o	25^o
Mold /Domain height (m)	2.152	2.152
Mold /Domain width (m)	1.83	0.965
Mold /Domain thickness (m)	0.238	0.238
Average inlet flow rate (m^3/s)	0.00344	0.00344
Average inlet speed (m/s)	1.69	1.69
Fluid density (kg/m^3)	1000	1000
Casting speed (m/s)	0.0152	0.0152
Fluid kinematic viscosity (m^2/s)	1.0×10^{-6}	1.0×10^{-6}
Particle inclusion size (mm)	2 – 3	3.8 (diameter)
Particle inclusion density (kg/m^3)	988	988
Corresponding alumina inclusion diameter in steel caster (μm)	300	300

Table 1: Experimental and simulation parameters.

Group index	Number of particles	Time of introduction
0	15000	0s – 1.6s
1	500	2s – 2.4s
2	500	4s – 4.4s
3	500	6s – 6.4s
4	500	8s – 8.4s
5	500	10s –10.4s

Table 2: Particle injection data.

This computation takes 19.2 CPUs per time step on a Pentium Ø 750MHz PC or 39 days for 175,000 time steps.

Particle Transport

The Lagrangian approach is employed for particle transport. The particle equation of motion is:

$$\mathrm{v}_{p,i} = \frac{dx_{p,i}}{dt} \tag{4}$$

$$\frac{d\mathrm{v}_{p,i}}{dt} = \frac{18\,r n_0}{r_p d_p^{\,2}}\left(1 + 0.15\mathrm{Re}_p^{\,0.687}\right)\left(\mathrm{v}_i - \mathrm{v}_{p,i}\right) + \left(1 - \frac{r}{r_p}\right) g_i \tag{5}$$

Proceedings of 2nd International Symposium on Turbulent and Shear Flow Phenomena, Vol. 2,
Royal Institute of Technology (KTH), Stockholm, Sweden, June 27 - 29, 2001, pp. 519-524.

where: $$\mathrm{Re}_p = \frac{\left|\vec{v}_p - \vec{v}\right| d_p}{n_0} \qquad (6)$$

The equations are integrated for each particle using a fourth order Runge-Kutta method at the same time as the velocity field is computed. This computation takes 2.4 additional CPUs per time step for 17500 particles or 5 additional days for 175000 time steps.

RESULTS AND DISCUSSION

Fluid Flow

Figure 2 shows a typical instantaneous velocity vector plot computed using LES. The flow emerges from the inlet port as a jet, diffuses as it traverses across the mold, impinges on the narrow face and splits into two recirculation regions consisting of the upper and lower rolls. This turbulent flow pattern is consistent with the experimental observations (Sussman, 1992; Thomas, 1994).

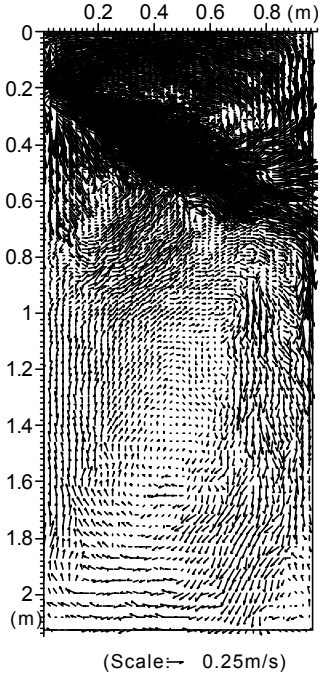

Figure 2: Computed typical instantaneous velocity field between wide faces.

Figures 3(a) and (b) show two typical instantaneous flow patterns of the upper roll. It is seen that the upper roll consists of a single large recirculation structure in Figure 3(a), but many distinct vortex structures in Figure 3(b). The upper roll alternates chaotically between these two extremes. This finding is consistent with a previous LES conducted for a 0.4-scale water model (Sivaramakrishnan, 2000). Only at the places very close to the top surface is the fluid velocity always horizontal. This finding is important in understanding the accuracy of the indirect measurement of the liquid steel velocity in caster mold using electromagnetic sensors.

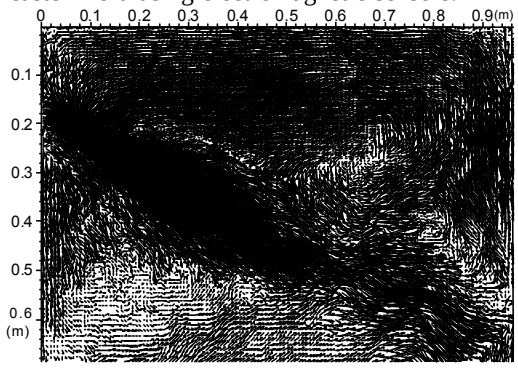

(a)

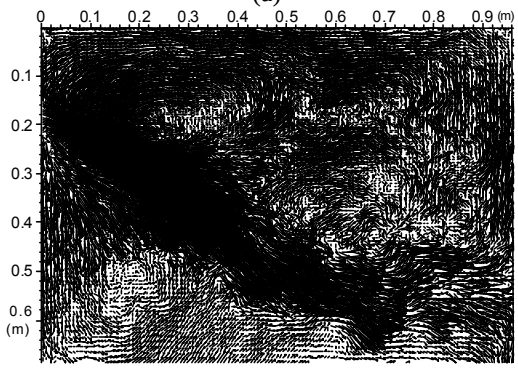

(b)

Figure 3: Instantaneous flow patterns in the upper roll.

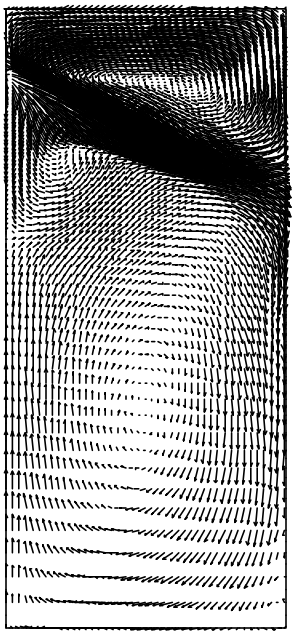

Figure 4: Time-averaged velocity field at the plane between wide faces.

Proceedings of 2nd International Symposium on Turbulent and Shear Flow Phenomena, Vol. 2,
Royal Institute of Technology (KTH), Stockholm, Sweden, June 27 - 29, 2001, pp. 519-524.

Figure 4 presents the time-averaged velocity field over a period of 100 seconds at the center plane between wide faces. A double-recirculation flow pattern is seen which is consistent with the instantaneous pictures and with previous PIV measurements and k-ε simulations (Sivaramakrishnan, 2000; Sussman, 1992; Thomas, 1994).

Figure 5 compares the computed and measured time-averaged fluid velocity (Thomas, 1994) along four vertical lines located at the center plane between wide faces and with different distances from the SEN. The computation generally agrees well with the measurements. The biggest discrepancy occurs at the line 460mm from the SEN, along which the computed maximum velocity occurs almost 0.1m deeper than the measurements. This might be generated by the uncertainties in the measurements. For example, the hot-wire anemometer was manually adjusted and hence likely not accurately placed to the desired position. The approximate inlet velocity field prescribed in the model may be an additional reason. It should be noted that significant differences exist between the measured time averages taken at different times.

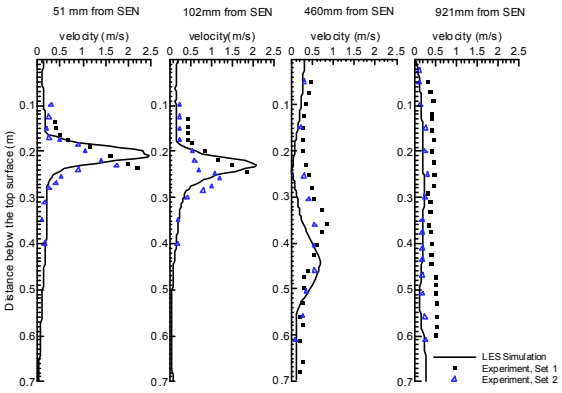

Figure 5: Comparison of the LES computation and measurements along four vertical lines.

Particle Transport

Figure 6 presents four snapshots of the distribution of the 15000 particles (group 0). These particles were evenly introduced into the domain over 1.6 seconds at a random position from the inlet port of the mold (as shown in Figure 9(a)) and with the initial velocity equal to the local instantaneous fluid velocity. The extended line inside the mold represents the position of the screen in the water model. The screen is used to capture particles and consequently help study the removal of particles to the top surface. The entrainment of particles by the screen is calculated by summing the particles that reach the top of the screen. The fluid flow and particle transport is not affected by the screen modeling.

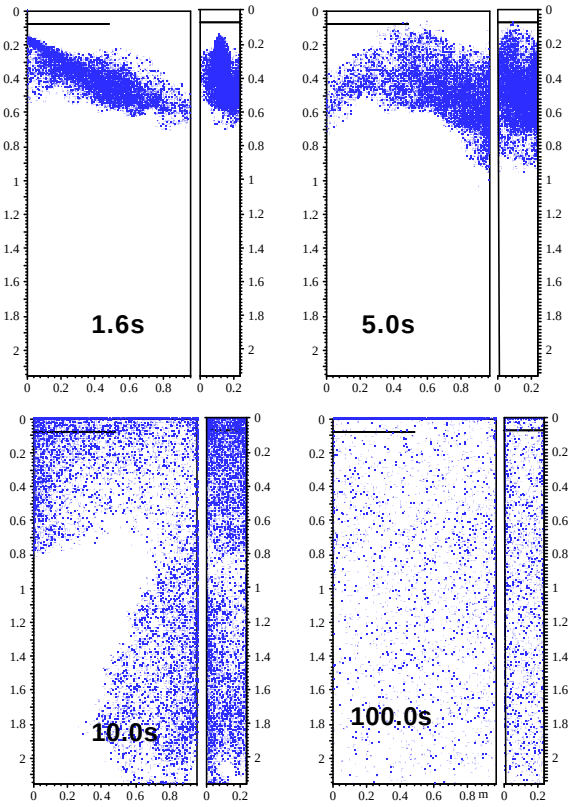

Figure 6: Distribution of the 15000 particles at four instants after their injection.

This figure shows that the particles move along the jet after injection (Figure 6(a)) and split into two parts (Figure 6(b)) corresponding to the upper and lower rolls when they hit the narrow face. Due in part to their buoyancy, some of the particles move to the top surface and are safely removed. Other particles flow out of the mold with the outflow and would be trapped at a deeper position, leading to defects in the real steel strand. Moreover, in a real steel caster, inclusion particles can also be entrapped by the solidifying shells (corresponding to the sidewalls of the water model). This was not modeled in the water model or LES.

The trajectory computations for the 15000-particle group (group 0) were processed to determine the computed particle removal rate to the top surface (lines) in Figure 7 and to compare the computed and measured removal rates by the screen (symbols) in the water model. Considering the approximate nature of the experiments, and uncertainties in the computations, the agreement between the computation and measurements appears to be quite good. The screen appears to simulate surface removal well at early times, but under-predicts it at later times (100s). The computation shows that the total removal rate

Proceedings of 2nd International Symposium on Turbulent and Shear Flow Phenomena, Vol. 2,
Royal Institute of Technology (KTH), Stockholm, Sweden, June 27 - 29, 2001, pp. 519-524.

appears to be very large (nearly 80%) when the walls are unable to trap particles.

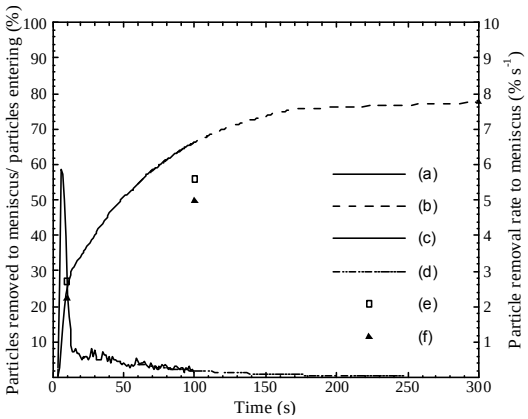

Figure 7: Particle removal to the top surface in full-scale water model: (a) particles removed to top surface (simulated); (b) particles removed to top surface (derived from extrapolation); (c) particle removal rate to top surface (derived from simulation); (d) particle removal rate to top surface (derived from extrapolation); (e) particles removed by screen, LES; (f) particles removed by screen, measurements.

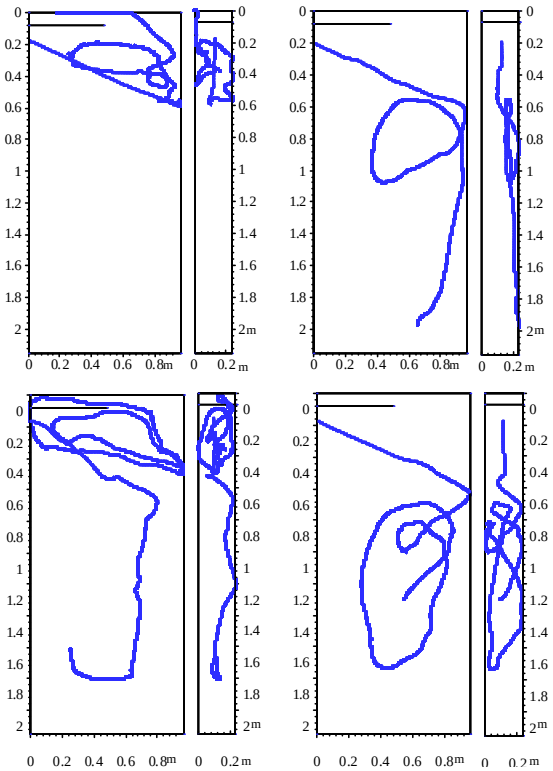

Figure 8: Four typical particle trajectories found in the computation.

Figure 8 shows four computed typical particle trajectories for 100 seconds or until they contact the top surface (the first picture) or exit the domain (the second picture). The last two particles are stilling moving. These irregular trajectories show some random motions and provide evidence for the effect of the turbulent fluid structures on particle transport.

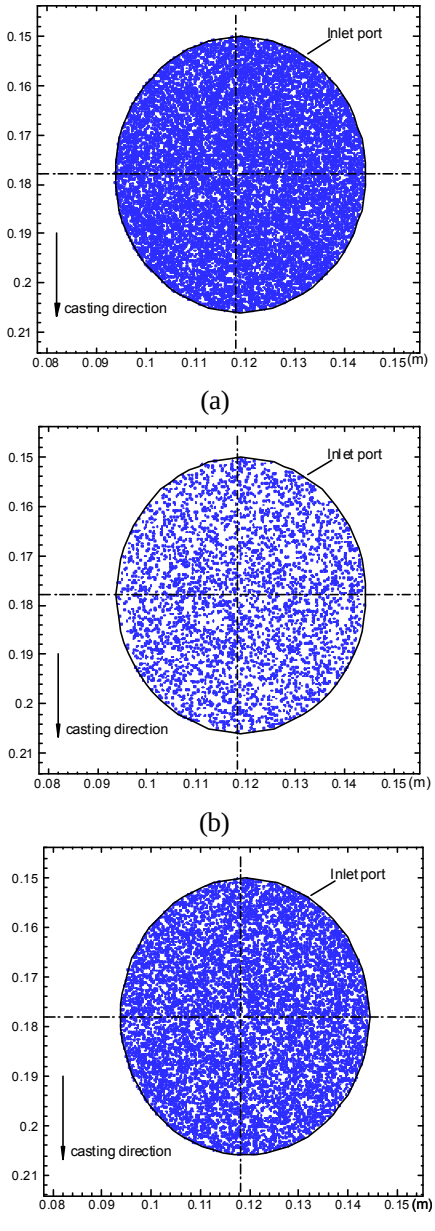

Figure 9: The initial positions of (a) the 15000 particles (group 0) and those in this particle group removed to the top surface in (b) 0-10 s and (c) 0-100 s after injection.

Figure 9(a) shows the initial positions of the 15000-particle group (group 0) at which they are introduced into the domain at the nozzle port exit plane. Figure 9(b) and (c) show those particles in this group removed to the top surface from 0 to 10 seconds and from 10 to 100 seconds respectively.

It is seen that particle removal to the top surface appears to be independent of its initial position. This is contrary to some expectations that particles exiting the top portion of the port might be more likely to be removed.

Finally, the computed particle removal by the screen for different particle groups and that of the measurements are compared in Table 3. It is found that the removal rate of an individual group of 500 particles can be very different by a factor of over 1.5. This appears to be due to the sensitivity of the particle trajectory to transient variations in the flow field which persist over several seconds. However the average of 5 groups agrees with both the experiment and the 15000-particle group result. This indicates that a large number of particles are required to study their transport (at least 2500 in this case), and that LES has the potential to accurately predict particle trajectories and removal.

CONCLUSIONS

The LES of the full-scale water model agrees with the measurements of fluid velocity and particle removal rate. Two typical turbulent flow structures are seen in the computation. Complex particle trajectories are seen in the computation, which agree with experimental observations, evidencing the important influence of the turbulence on particle transport. Particle removal to the top surface is found to be independent of the particle initial positions at the inlet port. Comparison of different particle groups shows that a large number of particles are required to study particle transport.

ACKNOWLEDGEMENTS

The authors thank the National Science Foundation (Grant DMI-98-00274) which made this research possible. The work is also supported by the member companies of the Continuous Casting Consortium at the University of Illinois at Urbana-Champaign.

NOMENCLATURE

$\frac{D}{Dt}$	total derivative ($=\frac{\partial}{\partial t}+\mathrm{v}_j\frac{\partial}{\partial x_j}$)
$\vec{x}$	displacement vector
$\vec{\mathrm{v}}$	velocity vector
n_0	laminar kinematic viscosity of fluid
n_{eff}	effective viscosity of fluid
Δx	mesh size in x direction
Δy	mesh size in y direction
Δz	mesh size in z direction
r	fluid density
r_p	particle material density

		0-10 seconds	10-100 seconds
LES	500 particle groups		
	1	27.2%	23.4%
	2	17.8%	27.2%
	3	26.2%	23.0%
	4	23.8%	23.2%
	5	33.0%	18.2%
	Average	25.56%	23.0%
	15000 particles (group 0)	26.96%	26.03%
Experiment		22.3%	27.6%

Table 3: Comparison of particle removal by screen.

d_p	particle diameter
t	time
$\vec{g}$	gravity vector

Subscripts:

i	directions (x, y, z)
p	particle

References

R. C. Sussman, M. T. Burns, X. Huang and B. G. Thomas, 1992, "Inclusion Particles Behavior in a Continuous Slab Casting Mold", *10th Process Technology Conference Proceedings*, Toronto, Ontario, pp. 291-304.

J. Smagorinsky, 1963, "General Circulation Experiments with the Primitive Equations. I. The Basic Experiment", *Monthly Weather Review*, vol. 91, pp. 99-164.

J. Robichaux, D. K. Tafti and S. P. Vanka, 1990, "Large Eddy Simulations of Turbulence on CM-2", *CFD 90-10*, Computational Fluid Dynamics Laboratory, Department of Mechanical and Industrial Engineering, University Illinois at Urbana-Champaign.

B. G. Thomas, X. Huang and R. C. Sussman, 1994, "Simulation of Argon Gas Flow Effects in a Continuous Slab Caster", *Metallurgical and Materials Transactions B*, vol. 25B, pp. 527-547.

S. Sivaramakrishnan, H. Bai, B. G. Thomas, S. P. Vanka, O. Dauby and M. Assar, 2000, "Transient Flow Structures in Continuous Casting of Steel", *Ironmaking Conference Proceedings*, vol. 59, Pittsburgh, PA, ISS, Warrendale, PA, pp. 542-557.